

Charged Higgs Search in 2HDM

Juxiang Li,^a Huayang Song,^b Shufang Su,^c Wei Su^a

^a*School of Science, Shenzhen Campus of Sun Yat-sen University, No. 66, Gongchang Road, Guangming District, Shenzhen, Guangdong 518107, P.R. China*

^b*Particle Theory and Cosmology Group, Center for Theoretical Physics of the Universe, Institute for Basic Science (IBS), Daejeon, 34126, Korea*

^c*Department of Physics, University of Arizona, Tucson, Arizona 85721, USA*

E-mail: lijx376@mail2.sysu.edu.cn, huayang@ibs.re.kr,
suwei26@mail.sysu.edu.cn, shufang@arizona.edu

ABSTRACT: In this paper, we present a comprehensive study of the collider search limits on the charged Higgses in the four types of Two Higgs Double Models (2HDM). In addition to constraints from flavor physics measurements, we include both the LEP charged Higgs search channels, as well as the LHC search results on the light and heavy charged Higgses. We consider both the conventional charged Higgs search channels of $H^\pm \rightarrow \tau\nu, cs, cb, tb$, and the latest search results on the exotic decay channels $H^\pm \rightarrow AW^\pm/HW^\pm$. We find that $H^\pm \rightarrow AW^\pm/HW^\pm$ are complementary to the conventional fermionic channels for $m_{H^\pm} < m_t$. For heavy H^\pm , $H^\pm \rightarrow AW^\pm/HW^\pm$ extend the reach of $\tan\beta$ beyond that of $H^\pm \rightarrow tb$ in the Type-L 2HDM. We also present the combined reach of all the neutral and charged Higgs searches.

KEYWORDS: Charged Higgs Boson

Contents

1	Introduction	1
2	Framework of the 2HDM	2
3	Experimental constraints	4
4	Higgs searches	7
4.1	Degenerate Higgs masses	7
4.2	Non-degenerate case	9
4.2.1	$\tan\beta$ vs. $m_{H^\pm} = m_H$	9
4.2.2	m_{H^\pm} vs. m_A	12
4.2.3	m_{H^\pm} vs. Δm_A	14
5	Conclusion	15

Contents

1 Introduction

Since the discovery of the 125 GeV Standard Model (SM)-like Higgs boson by the ATLAS [1] and CMS [2] collaborations at the Large Hadron Collider (LHC), the SM is confirmed to be a self-consistent theory at the electroweak scale. At the same time there are still unsolved puzzles in particle physics, such as the existence of dark matter, the baryon asymmetry of the universe, the strong CP problem, the muon $g - 2$ anomaly. These problems strongly motivate new physics beyond the Standard Model (BSM).

Many of the proposed new physics models contain an extended Higgs sector, among which the Two Higgs Doublet Model (2HDM) is one of the simplest extensions [3, 4]. After electroweak symmetry breaking (EWSB), the Higgs sector of the 2HDM consists of five physical Higgs bosons, including two CP-even neutral scalars h and H , a CP-odd Higgs boson A , and a pair of charged Higgs bosons H^\pm [4]. Studies of the existing constraints on the 2HDM charged Higgses have been performed in Ref. [5], focusing on the direct searches for charged Higgses at the LHC via conventional channels $H^\pm \rightarrow ff'$, as well as the indirect constraints of flavor physics for four different types of the 2HDM. However, the exotic channels $H^\pm \rightarrow W^\pm\phi$ ($\phi = A/H/h$) have been studied at the LEP ([6–8]), the LHC ([9–11]), as well as the future hadron colliders ([12, 13]). In the current study, we focus on the constraints on the charged Higgses including both the conventional channels and exotic decays of $H^\pm \rightarrow AW/HW$, for four different types of 2HDM.

If the mass of the charged Higgs m_{H^\pm} is less than the top quark mass m_t , the primary production channel of the charged Higgs is through top decay $t \rightarrow H^\pm b$. The charged Higgs boson primarily decays into $\tau\nu$ or cs , as well as Cabibbo–Kobayashi–Maskawa (CKM) suppressed channel cb . For heavier charged Higgs $m_{H^\pm} > m_t$, the main production mode is the top quark associated production $pp \rightarrow H^\pm tb$, with $H^\pm \rightarrow tb$ being dominant. Once kinematically accessible, the decays of $H^\pm \rightarrow AW/HW$ quickly dominate over the conventional search channels of $H^\pm \rightarrow ff'$. While the constraints from conventional channels relax, $H^\pm \rightarrow AW/HW$ provide alternative channels for the charged Higgs searches that are complementary to the conventional modes [9–13].

In this paper, we analyze the constraints on the charged Higgs boson from direct searches at the LHC and LEP, taking into account the latest experimental data. We also present an up-to-date analysis of the combined flavor constraints on the charged Higgs boson in the 2HDM, based on the latest flavor physics measurements [14–17] of the branching ratios of $B \rightarrow \chi_s \gamma$, $B_s \rightarrow \mu^+ \mu^-$, $B_d \rightarrow \mu^+ \mu^-$, $B \rightarrow \tau \nu$, $D_s \rightarrow \mu \nu$ and $D_s \rightarrow \tau \nu$ from the LHC and the B factories.

The rest of the paper is organized as follows. In Section 2, we introduce the theoretical framework of the 2HDM. In Section 3, we summarize the latest LHC and LEP searches that are relevant to charged Higgs studies, as well as flavor constraints. In Section 4, we present the constraints on the 2HDM parameter spaces of Type-I, Type-II, Type-L and Type-F. We conclude in Section 5.

2 Framework of the 2HDM

The most general Higgs potential of the CP-conserving 2HDM with a \mathcal{Z}_2 soft-breaking term is given by [4]

$$V = m_{11}^2 \Phi_1^\dagger \Phi_1 + m_{22}^2 \Phi_2^\dagger \Phi_2 - m_{12}^2 (\Phi_1^\dagger \Phi_2 + h.c.) + \frac{\lambda_1}{2} (\Phi_1^\dagger \Phi_1)^2 + \frac{\lambda_2}{2} (\Phi_2^\dagger \Phi_2)^2 + \lambda_3 (\Phi_1^\dagger \Phi_1) (\Phi_2^\dagger \Phi_2) + \lambda_4 (\Phi_1^\dagger \Phi_2) (\Phi_2^\dagger \Phi_1) + \frac{\lambda_5}{2} [(\Phi_1^\dagger \Phi_2)^2 + h.c.] , \quad (2.1)$$

in which the two complex hypercharge $Y = 1/2$, $SU(2)_L$ doublets are denoted as $\Phi_{1,2}$, and all the parameters are real. After the EWSB, the doublets can be parameterized as

$$\Phi_i = \begin{pmatrix} \phi_i^+ \\ (v_i + \phi_i^0 + i\varphi_i) / \sqrt{2} \end{pmatrix}, \quad i = 1, 2, \quad (2.2)$$

where $v_{1,2}$ are the vacuum expectation values of the neutral components which satisfy the condition $\sqrt{v_1^2 + v_2^2} \equiv v = 246$ GeV. For the purpose of this paper, the scalar sector of the 2HDM is parameterized by the physical Higgs mass (m_h, m_H, m_A and m_{H^\pm}), the mixing angle between the two CP-even Higgses (α), and the ratio of the two vacuum expectation values ($\tan \beta = v_2/v_1$), as well as a soft \mathcal{Z}_2 breaking parameter m_{12}^2 .

After the EWSB, the Higgs mass eigenstates contain a pair of CP-even Higgses h and H , a CP-odd Higgs A , and a pair of charged Higgses H^\pm through:

$$h = -s_\alpha \phi_1^0 + c_\alpha \phi_2^0, \quad H = c_\alpha \phi_1^0 + s_\alpha \phi_2^0, \quad (2.3)$$

$$A = -s_\beta \varphi_1 + c_\beta \varphi_2, \quad H^\pm = -s_\beta \phi_1^\pm + c_\beta \phi_2^\pm, \quad (2.4)$$

where we use the shorthand notation $s_x = \sin x$ and $c_x = \cos x$. In the following, we will identify h as the discovered 125 GeV Higgs. For general parameter choices, the exotic decay channels of the charged Higgs $H^\pm \rightarrow hW^\pm, H^\pm \rightarrow HW^\pm$ and $H^\pm \rightarrow AW^\pm$ can be kinematically accessible. The couplings governing these processes are given by

$$g_{H^\pm h W^\mp} = \frac{g c_{\beta-\alpha}}{2} (p_h - p_{H^\pm})_\mu, \quad g_{H^\pm H W^\mp} = \frac{g s_{\beta-\alpha}}{2} (p_H - p_{H^\pm})_\mu, \quad (2.5)$$

$$g_{H^\pm A W^\mp} = \frac{g}{2} (p_A - p_{H^\pm})_\mu, \quad (2.6)$$

where g is the $SU(2)_L$ coupling constant and p_i are the incoming momentum of the corresponding particle i . Higgs coupling measurements at the LHC prefer the alignment limit $s_{\beta-\alpha} = 1$. Therefore the coupling of the charged Higgs to the 125 GeV Higgs and the gauge boson is suppressed by $c_{\beta-\alpha} \sim 0$ and H^\pm is more likely to decay into the non-SM-like CP-even Higgs and a gauge boson HW^\pm or the CP-odd scalar and a gauge boson AW^\pm .

To avoid flavor-changing neutral currents (FCNC), one usually imposes a \mathcal{Z}_2 symmetry on the fermion and Higgs sectors, under which each fermion type only couples to one Higgs doublet. Depending on how fermions couple to $\Phi_{1,2}$, there are four possible types of 2HDMs: Type-I, Type-II, Type-L (lepton-specific) and Type-F (flipped), as shown in [Tab. 1](#).

2HDM	up-type	down-type	lepton	ξ_u	ξ_d	ξ_e
Type-I	Φ_2	Φ_2	Φ_2	$\cot \beta$	$\cot \beta$	$\cot \beta$
Type-II	Φ_2	Φ_1	Φ_1	$\cot \beta$	$-\tan \beta$	$-\tan \beta$
Type-L	Φ_2	Φ_2	Φ_1	$\cot \beta$	$\cot \beta$	$-\tan \beta$
Type-F	Φ_2	Φ_1	Φ_2	$\cot \beta$	$-\tan \beta$	$\cot \beta$

Table 1. Types of 2HDM, along with $\xi_{u,d,e}$ as defined in [Eq. \(2.7\)](#).

The Yukawa interactions [\[18\]](#) are expressed as

$$\begin{aligned}
-\mathcal{L}_Y^{int} = & \sum_{f=u,d,e} \frac{m_f}{v} \left(\xi_h^f \bar{f} f h + \xi_H^f \bar{f} f H - 2i I_f \xi_f \bar{f} \gamma_5 f A \right) \\
& + \frac{\sqrt{2}}{v} [V_{ud} \bar{u} (m_d \xi_d P_R - m_u \xi_u P_L) d H^+ + m_e \xi_e \bar{\nu} P_R e H^+ + h.c.],
\end{aligned} \quad (2.7)$$

where ξ_h^f and ξ_H^f are defined by

$$\xi_h^f = s_{\beta-\alpha} + \xi_f c_{\beta-\alpha}, \quad \xi_H^f = c_{\beta-\alpha} - \xi_f s_{\beta-\alpha}, \quad (2.8)$$

with $I_u = 1/2$, and $I_{d,e} = -1/2$. The values of $\xi_{u,d,e}$ in different types of 2HDM are shown in [Tab. 1](#). Given the difference in the fermion couplings under four different types, the results on the constrained parameter space based on the charged Higgs searches vary a lot.

3 Experimental constraints

In this chapter, we summarize the current available direct search results of the charged Higgs from the LHC and the LEP, as well as flavor measurements on B physics from the LHCb, BaBar and Belle.

Conventional channels: Conventional searches for the charged Higgs boson at the LHC focused on the decay into fermions: $H^\pm \rightarrow \tau\nu$ [19–29], cs [30–33], cb [34, 35] and tb [27, 36–41], which are collected in Tab. 2. Measurements of the non-resonant search of the SM process $t\bar{t}b\bar{b}$ have been performed at both ATLAS and CMS [42–49], along with modeling studies [50–52] since it gives irreducible background to the top pair associated Higgs boson production ($t\bar{t}H/A$) with $H/A \rightarrow b\bar{b}$. We note that such continuum measurement can constrain the tbH^\pm production with $H^\pm \rightarrow tb$ as well, especially when the width of the charged Higgs is large such that resonant search becomes ineffective. The current experimental constraints on the $t\bar{t}b\bar{b}$ channel depends on the definitions of their fiducial phase space regions which usually involves some non-trivial cuts. Therefore, without detailed collider analyses it is difficult to reinterpret these constraints on the parameter space of a charged Higgs. However, we want to emphasize that such an analysis may be powerful, similar to the impact of continuum $t\bar{t}t\bar{t}$ analysis on the neutral scalar searches [53].

channel	ATLAS			CMS		
	7 TeV	8 TeV	13 TeV	7 TeV	8 TeV	13 TeV
$H^\pm \rightarrow \tau\nu$	[19, 20]	[21]	[22, 23]	[24]	[25–27]	[28, 29]
$H^\pm \rightarrow cs$	[30]	-	[33]	-	[31]	[32]
$H^\pm \rightarrow cb$	-	-	[34]	-	[35]	-
$pp \rightarrow tbH^\pm \rightarrow t\bar{t}b\bar{b}$	-	[36]	[37, 38]	-	[27, 39]	[40, 41]

Table 2. Charged Higgs searches with $H^\pm \rightarrow ff'$ at the LHC.

Exotic decays channels: The exotic decay channels $H^\pm \rightarrow W^{\pm(*)}\phi$ ($\phi = A/H/h$) open when the mass of the charged Higgs is greater than the mass of the neutral Higgs. The current searches results at the LHC for $H^\pm \rightarrow AW^\pm/HW^\pm$ are very limited, as listed in Tab. 3. For the light charged Higgs, CMS results are only given for the cases $m_{H^\pm} = m_A + 85$ GeV with a luminosity of 35.9 fb^{-1} [54], while ATLAS only lists the results for $m_{H^\pm} = 120, 140, 160$ GeV with a luminosity of 139 fb^{-1} [55]. Both collaborations focus on the final states of $W\mu\mu$. For the heavy charged Higgs, CMS also performed a search with an integrated luminosity of 138 fb^{-1} in the $H^\pm \rightarrow W^\pm H \rightarrow W\tau\tau$ channel assuming $m_H = 200$ GeV [56].

LEP searches: Searches for the charged Higgs bosons have been performed at the LEP, mainly using the H^\pm -pair production $e^+e^- \rightarrow H^+H^-$, since the cross section for $e^+e^- \rightarrow H^\pm W^\mp$ is suppressed [57]. In the 2HDM, the production cross section of charged Higgs boson pair is completely determined at the tree-level by the charged Higgs boson mass and

mass	channel	ATLAS	CMS
		13TeV	13TeV
$m_{H^\pm} < m_t$	$H^\pm \rightarrow AW \rightarrow W\mu\mu$	[55]	[54]
$m_{H^\pm} > m_t$	$H^\pm \rightarrow HW \rightarrow W\tau\tau$	-	[56]

Table 3. Charged Higgs searches with $H^\pm \rightarrow HW/AW$ at the LHC.

known SM parameters [58]. The limits on the charged Higgs boson mass are robust when all relevant charged Higgs boson decay channels are considered. Combining data from the four collaborations ALEPH [59], DELPHI [60], L3 [61], and OPAL [62] on $H^\pm \rightarrow \tau\nu$ and $H^\pm \rightarrow cs$ channels, a limit of $m_{H^\pm} \geq 80$ GeV is obtained under the assumption that $H^\pm \rightarrow AW^\pm$ is absent. The DELPHI [63] and OPAL [64] collaborations also searched for $H^\pm \rightarrow AW^\pm$. In the Type-I 2HDM, for $m_A = 12$ GeV, a limit of $m_{H^\pm} \geq 72.5$ GeV is obtained [8]. In this work we use LEP limits from the $\tau\nu$ final state and the cs final state, and the OPAL limits from the AW^\pm channel, with data obtained from **HiggsBounds** [65–70].

Observable	Experimental result	SM prediction
R_γ	$(3.22 \pm 0.15) \times 10^{-3}$ [71]	$(3.35 \pm 0.16) \times 10^{-3}$ [72]
$BR(B \rightarrow \chi_s \gamma)$	$(3.32 \pm 0.15) \times 10^{-4}$ [14]	$(3.40 \pm 0.17) \times 10^{-4}$ [72]
$BR(B \rightarrow \tau\nu)$	$(1.094 \pm 0.208) \times 10^{-4}$ [15]	$(9.24 \pm 1.13) \times 10^{-5}$ [73]
$BR(B_s \rightarrow \mu^+ \mu^-)$	$(3.34 \pm 0.27) \times 10^{-9}$ [16]	$(3.64 \pm 0.12) \times 10^{-9}$ [74]
$BR(B_d \rightarrow \mu^+ \mu^-)$	$(0.6 \pm 0.7) \times 10^{-10}$ [17]	$(1.03 \pm 0.05) \times 10^{-10}$ [17]
$BR(D_s \rightarrow \tau\nu)$	$(5.33 \pm 0.12) \times 10^{-2}$ [15]	$(5.22 \pm 0.04) \times 10^{-2}$ [73]
$BR(D_s \rightarrow \mu\nu)$	$(5.36 \pm 0.12) \times 10^{-3}$ [15]	$(5.31 \pm 0.04) \times 10^{-3}$ [73]
$R(D)$	(0.342 ± 0.026) [15]	(0.303 ± 0.006) [73]

Table 4. Experimental results for flavor physics observables and their corresponding SM predictions.

Flavor constraints: One of the most stringent constraints on the 2HDM comes from the precision measurements of flavor physics observables, especially the inclusive decay $B \rightarrow \chi_s \gamma$. At $E_0 = 1.6$ GeV, the experimental world average for $BR(B \rightarrow \chi_s \gamma)$ is $(3.32 \pm 0.15) \times 10^{-4}$ [14], and $R_\gamma^{exp} = B_{(s+d)\gamma}/B_{cl\nu} = (3.22 \pm 0.15) \times 10^{-3}$ [71]. The latest update of the SM values at the NNLO in QCD are [72],

$$BR(B \rightarrow \chi_s \gamma)^{SM} = (3.40 \pm 0.17) \times 10^{-4}, \quad R_\gamma^{SM} = (3.35 \pm 0.16) \times 10^{-3}. \quad (3.1)$$

We also investigate the constraints on the charged Higgs from other flavor physics observations. Both the experimental measurements and their corresponding SM predictions are collected in Tab. 4. Employing the method outlined in Ref. [72], we calculate the theoretical value of R_γ and $BR(B \rightarrow \chi_s \gamma)$ in the 2HDM. In addition, we use the **SuperIso** [75–77] to calculate the other flavor observables in the 2HDM.

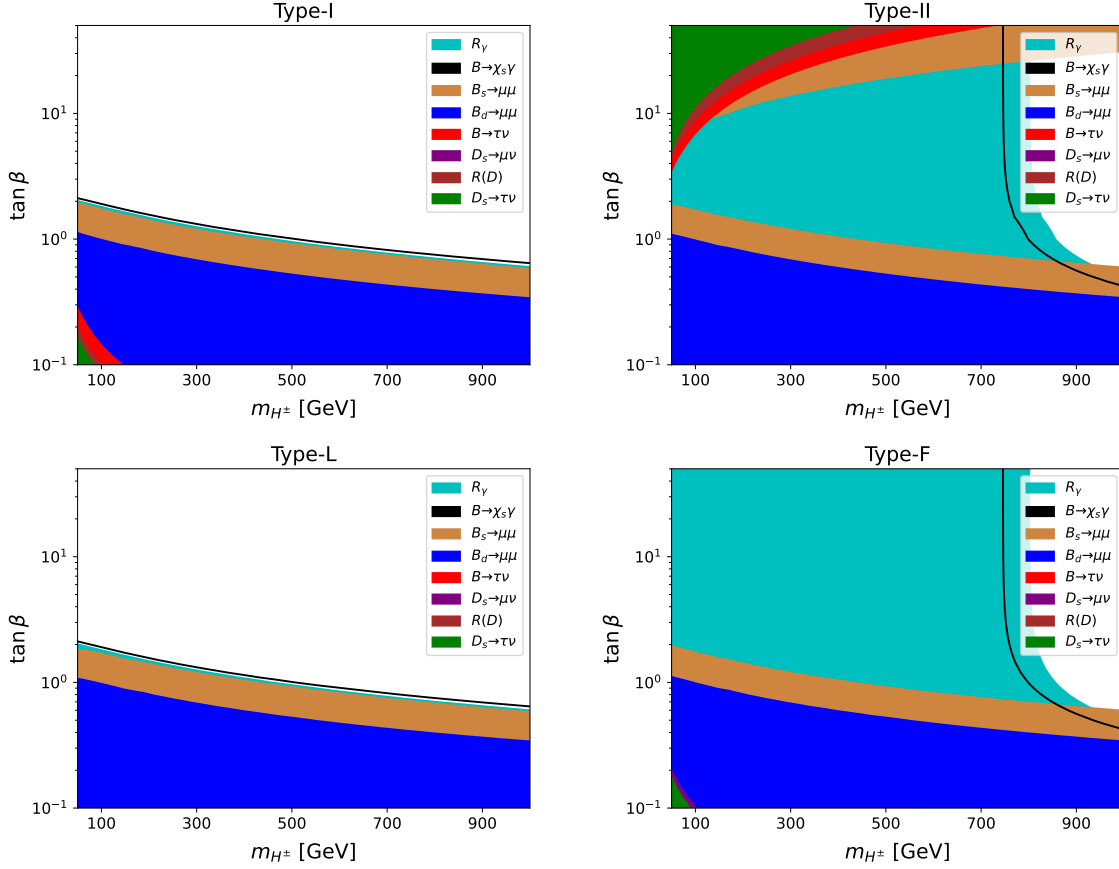


Figure 1. 95% C.L. contour plots of the allowed parameter space in the m_{H^\pm} vs. $\tan\beta$ plane for Type-I 2HDM (upper left), Type-II 2HDM (upper right), Type-L 2HDM (lower left) and Type-F 2HDM (lower right) under flavor constraints.

In Figure 1, we present the flavor constraints on different types of 2HDM. For the Type-I 2HDM (upper left panel), $B \rightarrow \chi_s \gamma$ constraints are sensitive only to low $\tan\beta$ around 2 or less, given that all fermion couplings are proportional to $1/\tan\beta$. For the Type-II 2HDM (upper right panel), the measurements of $R_\gamma = B_{(s+d)\gamma}/B_{cl\bar{\nu}}$ impose a very strong constraint on the Type-II 2HDM, leading to a lower limit on the mass of the charged Higgs particle to be around 800 GeV. For the Type-L (Type-F) 2HDM, the strongest constraints imposed by flavor physics on the charged Higgs are similar to those of Type-I (Type-II). Even though in the Type-II and Type-F 2HDM, charged Higgs mass less than about 800 GeV has been tightly constrained by the flavor measurements, in our collider analyses below, we consider all ranges of charged Higgs mass as an independent approach for the charged Higgs sector.

Precision constraints. Electroweak precision measurements [78] require the mass of the charged Higgs to be close to the mass of one of the neutral Higgses, $m_{H^\pm} \sim m_H$ or m_A [79]. In our analyses below, we take the assumption of $m_{H^\pm} = m_H$ to satisfy the electroweak

precision constraints. The case where $m_{H^\pm} = m_A$ can be analyzed similarly.

4 Higgs searches

To interpret the experimental results, we take the experimental upper limits on the cross sections multiplied by the branching fractions $\sigma \times BR$ for various channels, as well as SM-like Higgs precision measurements and Γ_{H^\pm} to directly constrain the 2HDM parameter space. We use the **prospino** [80, 81] package to calculate the charged Higgs production cross sections in the 2HDM at the NLO level and the **2HDMC** [82] to calculate the Higgs decay branching fractions.

4.1 Degenerate Higgs masses

In Figure 2, we show the constraints from direct searches for charged Higgs bosons at the LHC in the m_{H^\pm} vs. $\tan\beta$ plane for four different types of the 2HDM under the alignment limit of $c_{\beta-\alpha} = 0$. The Z_2 soft-break parameter m_{12}^2 is chosen to be $m_{12}^2 = m_H^2 s_\beta c_\beta$ to satisfy the theoretical constraints such as unitarity and vacuum stability conditions. We assume a degenerate BSM Higgs spectrum $m_{H^\pm} = m_H = m_A$ such that electroweak precision constraints are automatically satisfied and the exotic decay channels do not open. The results are independent of $c_{\beta-\alpha}$ in the case of degenerate Higgs mass spectrum.

For the Type-I 2HDM (upper left panel), the couplings of charged Higgs and fermions are proportional to $1/\tan\beta$. The charged Higgs productions, in low mass region of $m_{H^\pm} < m_t$ via top decay $t \rightarrow bH^\pm$ and large mass region of $m_{H^\pm} > m_t$ via tbH^\pm associated production, are both suppressed at large $\tan\beta$. Therefore, only relatively small $\tan\beta$ region is constrained by the direct searches. In the low mass region, $H^\pm \rightarrow \tau\nu$ dominates, while the branching fraction of $H^\pm \rightarrow cs$ is about a factor of two smaller. The branching fraction of $H^\pm \rightarrow cb$ is suppressed by more than an order of magnitude. The dominant decay channel of $H^\pm \rightarrow \tau\nu$ provides the most sensitive reach given the relatively clean final state, excluding $\tan\beta < 20$. Note that the low mass region is extended down to 60 GeV in the recent results from channel $H^\pm \rightarrow cb$ [34] and $H^\pm \rightarrow cs$ [33]. In the high mass region, H^\pm dominantly decays to tb , suppressing the decay branching fractions of other decay channels by at least four orders of magnitude. Therefore, $H^\pm \rightarrow tb$ provides the best limit of $\tan\beta \lesssim 1 - 2$ for $m_{H^\pm} < 1$ TeV. The slightly weaker constraint on the $tbH^\pm \rightarrow ttbb$ channel around $m_{H^\pm} = 800$ GeV is due to upward fluctuation of the experimental data at that particular point [38]. We also show the region corresponding to $\Gamma/m_{H^\pm} > 0.1$ (hatch line), in which the resonant search results are not applicable given the large charged Higgs decay width. Furthermore, LEP [59–64] excludes a charged Higgs with mass up to 83 GeV via $e^+e^- \rightarrow H^+H^-$ production channel.

For the Type-II 2HDM (upper right panel), the charged Higgs couplings are proportional to $\tan\beta$ for the down quark-type Yukawa coupling, and $1/\tan\beta$ for the up quark-type Yukawa. The productions of charged Higgs via $t \rightarrow H^\pm b$ for small m_{H^\pm} and tbH^\pm for large m_{H^\pm} are enhanced for both small and large $\tan\beta$. For the light H^\pm , $H^\pm \rightarrow \tau\nu$ dominates at almost 100% branching fraction, which excludes $m_{H^\pm} < m_t$ at almost all values of $\tan\beta > 0.2$. The

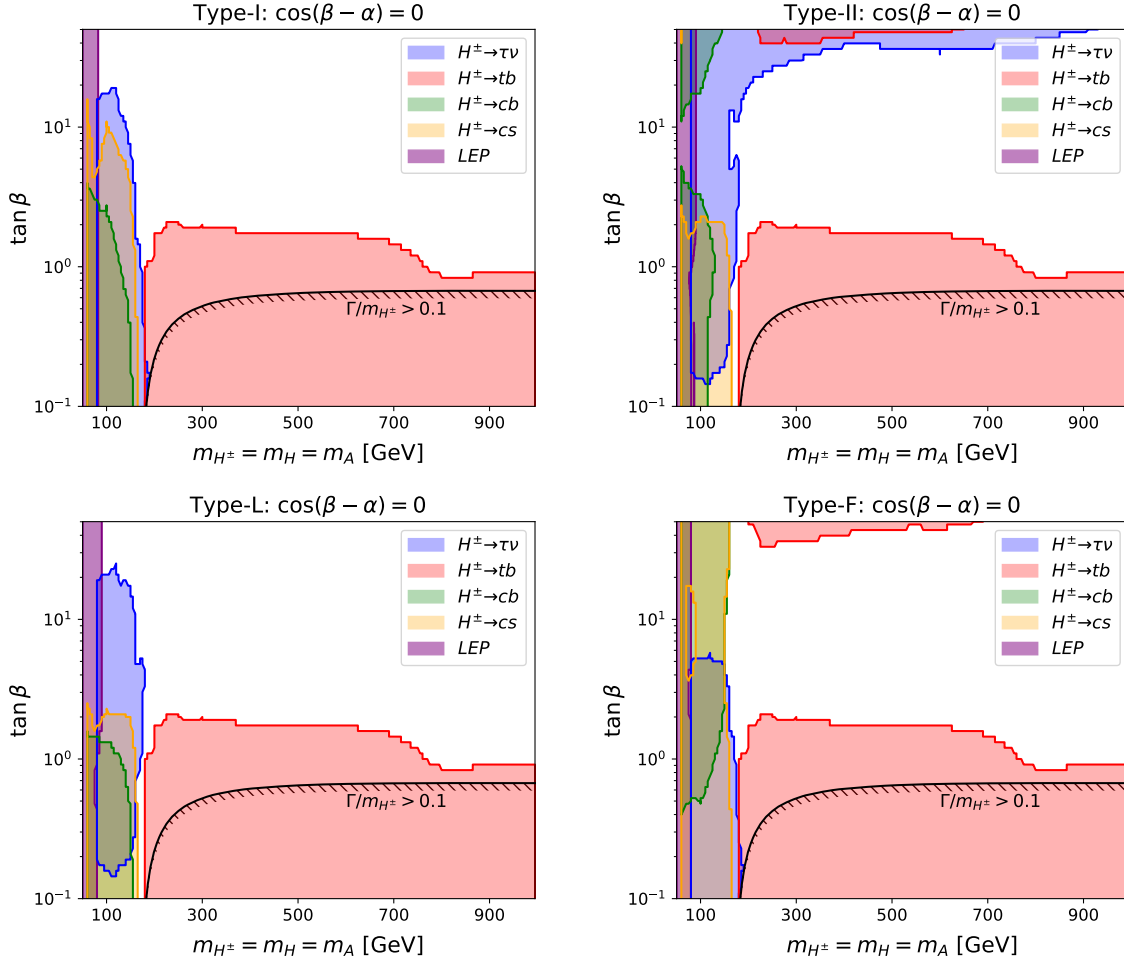


Figure 2. The 95% C.L. exclusion regions in the m_{H^\pm} vs. $\tan\beta$ plane in the Type-I 2HDM (upper left), Type-II 2HDM (upper right), Type-L 2HDM (lower left) and Type-F 2HDM (lower right) with the degenerate mass spectrum of $m_{H^\pm} = m_H = m_A$ under alignment limit, taking into account i) the theoretical calculations of the charged Higgs width $\Gamma/m_{H^\pm} > 0.1$ (hatch line); ii) the conventional search results at the LHC via $H^\pm \rightarrow \tau\nu$ (blue), $H^\pm \rightarrow cb$ (green), $H^\pm \rightarrow cs$ (orange), and $tbH^\pm \rightarrow ttbb$ (red); iii) LEP limits on the charged Higgs (purple).

branching fraction of $H^\pm \rightarrow cb$ is larger than that of cs , which provides a better reach at small $\tan\beta$, and also provides a certain exclusion at large $\tan\beta$ with the enhanced production rate from $t \rightarrow H^\pm b$. In the heavy H^\pm case, while the small $\tan\beta$ exclusion is similar to that of the Type-I case via $H^\pm \rightarrow tb$, $H^\pm \rightarrow \tau\nu$ provides a better reach at large $\tan\beta$ with the branching fraction of such channel being about 10%. For $\tan\beta > 30$ (40), the mass of charged Higgs m_{H^\pm} has been excluded up to 315 (805) GeV. $H^\pm \rightarrow tb$ channel can also exclude a portion of the parameter space at very large values of $\tan\beta \sim 50$.

For the Type-L 2HDM (lower left panel), the couplings between the charged Higgs and

quarks are the same as for the Type-I 2HDM, inversely proportional to the $\tan\beta$ value. Consequently, the production cross-section of the charged Higgs is suppressed at large values of $\tan\beta$ as in the Type-I 2HDM case. The coupling of the H^\pm to $\tau\nu$, however, is proportional to $\tan\beta$. Therefore, the decays of $H^\pm \rightarrow cb$ and $H^\pm \rightarrow cs$ are significantly suppressed with respect to the Type-I 2HDM when $\tan\beta \gtrsim 1$. The excluded region via $H^\pm \rightarrow \tau\nu$ is similar to the Type-II at small $\tan\beta$. For larger $\tan\beta$, there is no excluded region through the $\tau\nu$ channel since the production cross-section of the charged Higgs is heavily suppressed.

For the Type-F 2HDM (lower right panel), the couplings between the charged Higgs and quarks are the same as in the Type-II model, while the leptonic couplings are proportional to $1/\tan\beta$. Therefore, the production cross section of the charged Higgs is enhanced at both small and large $\tan\beta$. In the low mass region, the decay branching fraction of $H^\pm \rightarrow cs$ is around $0.2 - 0.4$ for all values of $\tan\beta$, which provides limits across all the values of $\tan\beta$. The decay mode of H^\pm to cb is significantly suppressed at small values of $\tan\beta$, while $H^\pm \rightarrow \tau\nu$ decay dominates. However, when $\tan\beta$ exceeds 5, the decay channel $H^\pm \rightarrow cb$ becomes the dominant one, while the $H^\pm \rightarrow \tau\nu$ channel is significantly suppressed. Therefore, $H^\pm \rightarrow \tau\nu$ excludes light H^\pm up to $\tan\beta \sim 5$ while $H^\pm \rightarrow cb$ excludes light H^\pm for $\tan\beta > 0.4$. For the heavy H^\pm , the exclusion region is similar to that of the Type-II case via $H^\pm \rightarrow tb$, while $H^\pm \rightarrow \tau\nu$ exclusion disappears at large $\tan\beta$.

4.2 Non-degenerate case

Once there are mass splittings between the charged Higgs and neutral Higgs masses, additional exotic channels such as $H^\pm \rightarrow AW/HW$ open and rapidly dominate the decay. Therefore, the reaches of the conventional searches shown earlier are reduced. At the same time, the exotic decay channels $H^\pm \rightarrow AW/HW$ provide alternative possibilities for charged Higgs searches at the LHC. In our analysis below, we assume that $m_{H^\pm} = m_H$ to satisfy the electroweak precision constraints. $H^\pm \rightarrow HW$ is therefore kinematically closed and our results are independent of $c_{\beta-\alpha}$. Once we relax the degenerate mass relation of $m_{H^\pm} = m_H$, $H^\pm \rightarrow HW$ could be kinematically accessible as well, which will introduce $c_{\beta-\alpha}$ dependence. Similar analyses can be performed under the assumption of $m_{H^\pm} = m_A$ or more general spectrum of m_{H^\pm} , m_H and m_A , as long as electroweak precision constraints are satisfied. Our analyses below under the assumption of $m_{H^\pm} = m_H$ nevertheless show the general features of the complementarity between such exotic channels and the conventional charged Higgs search channels.

4.2.1 $\tan\beta$ vs. $m_{H^\pm} = m_H$

In Figure 3, we show the current collider limits [54] in the 2HDM on the m_{H^\pm} vs. $\tan\beta$ plane, assuming that $\Delta m_A = m_{H^\pm} - m_A = 85$ GeV in which the charged Higgs mass is just above the kinematic threshold of the decay mode $H^\pm \rightarrow AW$ (brown). The experimental results are only available for $m_{H^\pm} < m_t$. Gray area indicates the nonphysical regions with negative values of m_A .

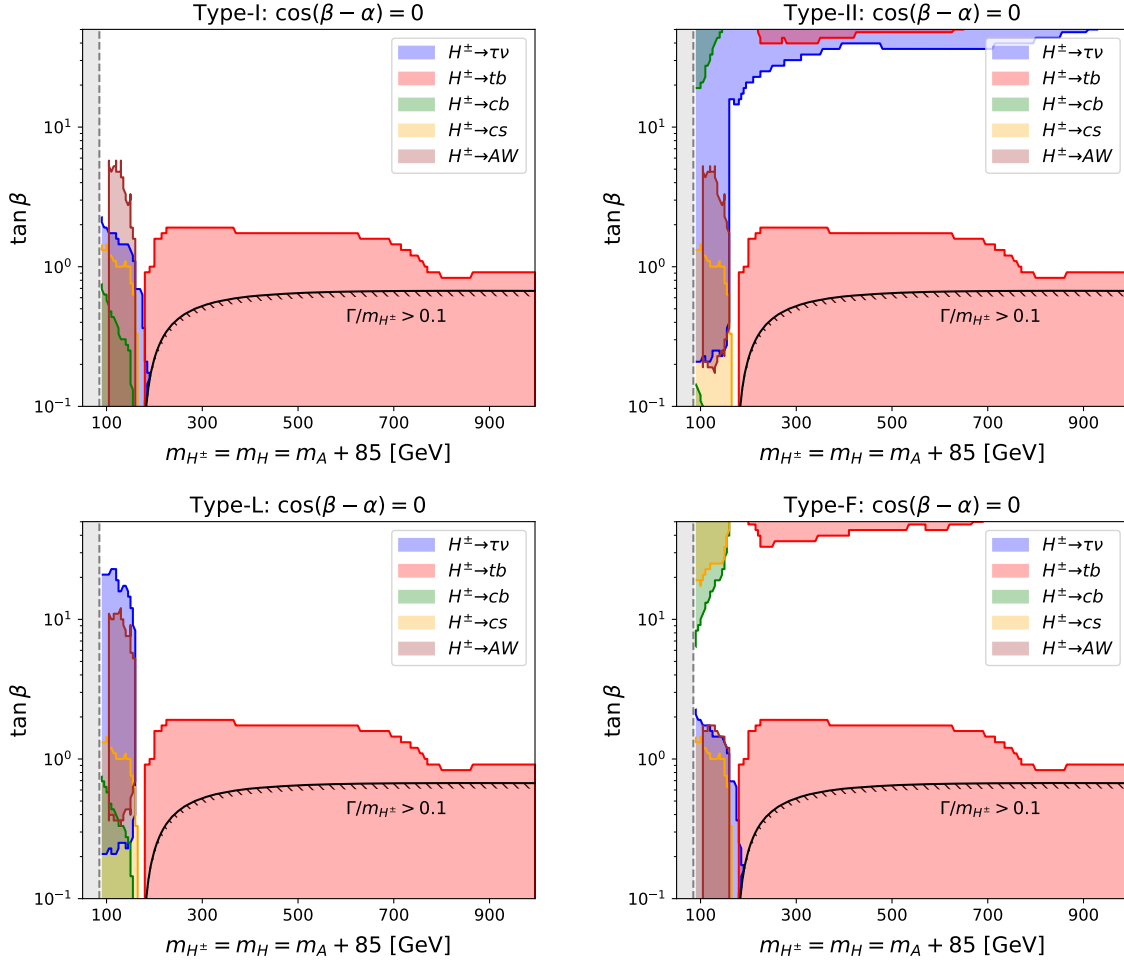


Figure 3. The 95% C.L. exclusion regions in the m_{H^\pm} vs. $\tan\beta$ plane of the Type-I 2HDM (upper left), Type-II 2HDM (upper right), Type-L 2HDM (lower left) and Type-F 2HDM (lower right) with $\Delta m_A = m_{H^\pm} - m_A = 85$ GeV. The constraints from $H^\pm \rightarrow AW$ is indicated in brown. Gray area indicates the nonphysical regions with negative values of m_A . The rest of color coding is the same as Figure 2.

For the Type-I 2HDM (upper left panel), $H^\pm \rightarrow AW$ provides the strongest constraint for the light H^\pm case with an upper limit of $\tan\beta$ around 6. The reaches of $\tau\nu$, cs and cb channels are suppressed, comparing to those in the degenerate case. Once $H^\pm \rightarrow tb$ opens up, it still dominates at small $\tan\beta$, with a collider reach similar to that in the degenerate case.

For the Type-II and Type-L 2HDM (upper right and lower left panels), with a mass difference of 85 GeV between m_{H^\pm} and m_A , $H^\pm \rightarrow \tau\nu$ dominates over AW channel for $\tan\beta \gtrsim 5$. Therefore, the limit plots are very similar to those in the degenerate case, with only the addition of $H^\pm \rightarrow AW$ reach at light H^\pm , and the suppression of the reaches of

$H^\pm \rightarrow cs, cb$. Note that the reach of the AW channel only extends to $\tan \beta \sim 0.2(0.4)$ for the Type-II (-L) 2HDM. This is due to the suppression of decay channel $A \rightarrow \mu\mu$ in the Type-II (-L) 2HDM at small $\tan \beta$ for $A(\rightarrow \mu\mu)W$ channel.

For the Type-F 2HDM (lower right panel), the reaches from $H^\pm \rightarrow \tau\nu, cs$ and cb at small m_{H^\pm} are suppressed comparing to those in the degenerate case due to the opening of $H^\pm \rightarrow AW$. The reach of $H^\pm \rightarrow AW$, however, is reduced at $\tan \beta \gtrsim 2$ given the suppression of $A \rightarrow \mu\mu$. For the heavy H^\pm , the exclusion region of the tb channel is similar to that of the degenerate case.

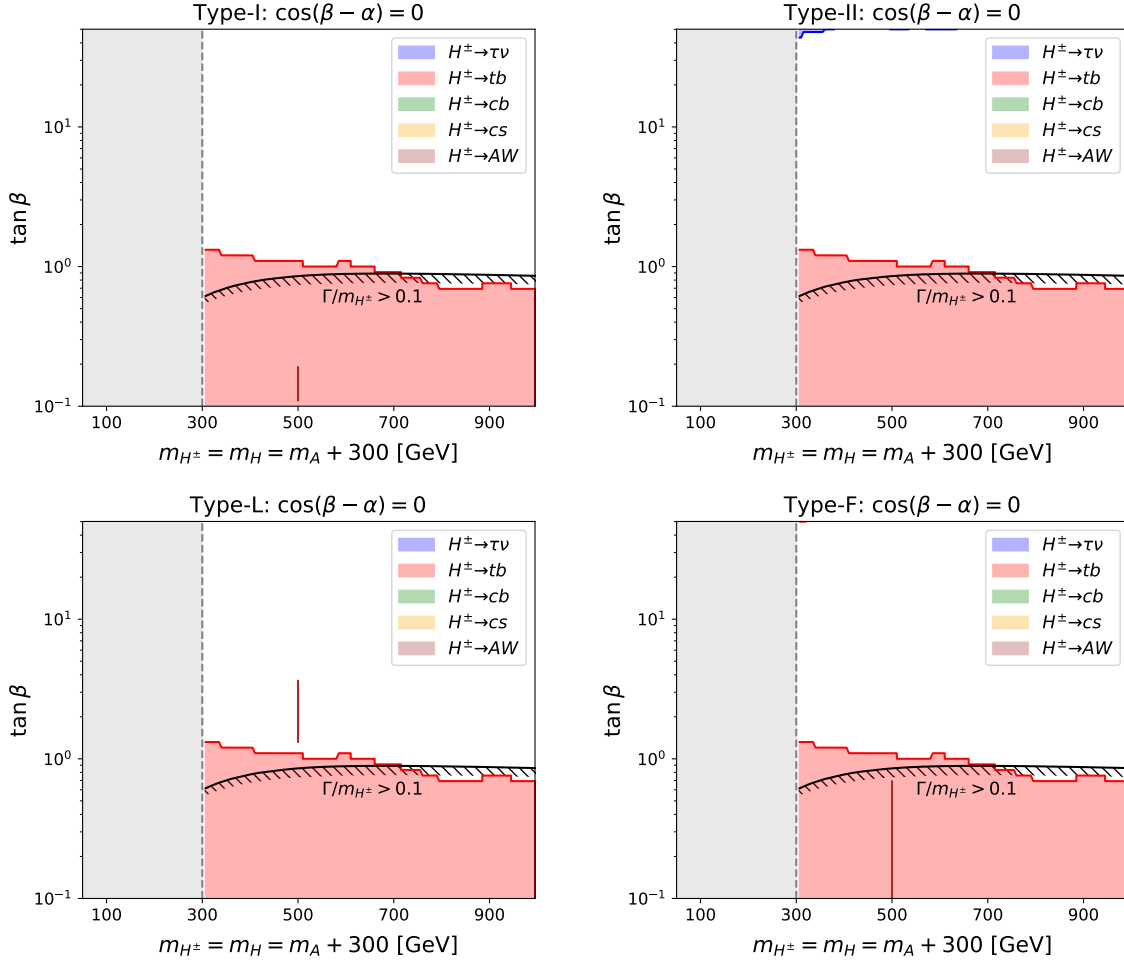


Figure 4. The 95% C.L. exclusion regions in the m_{H^\pm} vs. $\tan \beta$ plane of the Type-I 2HDM (upper left), Type-II 2HDM (upper right), Type-L 2HDM (lower left) and Type-F 2HDM (lower right) with $\Delta m_A = m_{H^\pm} - m_A = 300$ GeV. Color coding is the same as Figure 3.

In Figure 4, we show the current collider limits in the $m_{H^\pm} = m_H$ vs. $\tan \beta$ plane of four different types of 2HDM with $\Delta m_A = m_{H^\pm} - m_A = 300$ GeV. $m_{H^\pm} < 300$ GeV is nonphysical for such Δm_A . Note that the experimental limits of $H^\pm \rightarrow AW$ channel for $\Delta m_A \neq 85$ GeV

are only given for a fixed value of $m_A = 200$ GeV [56] for $m_{H^\pm} > m_t$. Once $\Delta m_A \gtrsim 100$ GeV, $H^\pm \rightarrow AW$ quickly dominates over the fermionic decay channels. Therefore, the reach of $H^\pm \rightarrow tb$ channel at large m_{H^\pm} is suppressed comparing to that in the degenerate case, as shown by the red regions in all panels.

The best reach of $H^\pm \rightarrow AW$ is obtained in the Type-L 2HDM for $\tan\beta$ between 1 to 5, given the enhanced decay branching fraction of $A \rightarrow \tau\tau$. For the Type-I and Type-F, the reach via $H^\pm \rightarrow AW$ is less comparing to that via $H^\pm \rightarrow tb$. There is no limit obtained from $H^\pm \rightarrow AW$ in the Type-II 2HDM due to the suppression of $A \rightarrow \tau\tau$ channel at small $\tan\beta$. For larger mass splitting of Δm_A , the reach of $H^\pm \rightarrow tb$ is further suppressed, while the reach of $H^\pm \rightarrow AW$ slightly increases. However, the feature remains similar to the case of $\Delta m_A = 300$ GeV.

4.2.2 m_{H^\pm} vs. m_A

In Figure 5, we show the LHC collider search limits in the m_{H^\pm} vs. m_A plane for $\tan\beta = 1.5$. In the top four panels we only take into account the charged Higgs searches. Other than the region around $m_{H^\pm} \sim m_t$, which has a narrower gap in the Type-II and Type-L 2HDM due to the coverage from $H^\pm \rightarrow \tau\nu$, the exclusion regions of the conventional channels in all the four types of 2HDM are very similar. The fermionic decays of H^\pm almost cover all regions of $m_{H^\pm} \lesssim 715$ GeV for $m_{H^\pm} < m_A + m_W$, except for $m_{H^\pm} \sim m_t$.

The gray diagonal line indicates $m_{H^\pm} = m_A + m_W$, below which the on-shell decay of $H^\pm \rightarrow AW$ is kinematically open. The $H^\pm tb$ associated production with $H^\pm \rightarrow tb$ extends the reach beyond $\Delta m_A = m_W$. Once $H^\pm \rightarrow AW$ is kinematically accessible, it provides the largest decay branching ratio of the charged Higgs, in particular for heavy H^\pm . The horizontal brown dashed line indicates $m_A = 200$ GeV, which is the benchmark value of m_A that is chosen for the $H^\pm \rightarrow AW$ search in the heavy H^\pm case. For the Type-L, $H^\pm \rightarrow AW$ provides the best charged Higgs search limit. For the Type-I, -II, and -F, the reach of $H^\pm \rightarrow AW$ is severely suppressed due to the small branching ratio of $A \rightarrow \tau\tau$ at low $\tan\beta$.

The bottom two panels show the exclusion reaches in the Type-L and -F including the collider search limits on the neutral scalar A as well [53], which are indicated by the horizontal exclusion bands. $A \rightarrow \tau\tau$ [83–86] and $\gamma\gamma$ [87–93] dominate the reach below $2m_t$, while $A \rightarrow tt$ [94, 95] provides the best reach for $400 \text{ GeV} < m_A < 580 \text{ GeV}$. For the very small value of m_A , we include the limits from $h \rightarrow AA$ [96–110] as well. Note that if we impose the relation of $m_{H^\pm} = m_H$, additional constraints from H searches (indicated by vertical bands), as well as $A \rightarrow ZH$ [111–116] and $H \rightarrow AZ$ [111–115] also show up, which are indicated by the vertical and horizontal cyan region. $A/H \rightarrow HZ/AZ$ searches exclude regions of $m_{H/A}$ between 30 to 450 GeV. Exclusions for the Type-I (II) are similar to those of the Type-F (L) from these additional A and H search modes.

We also show the case of $\tan\beta = 5$ in Figure 6. Comparing to the $\tan\beta = 1.5$ case, the limits get weaker given the reduced production cross section of the charged Higgs. Only limits from $H^\pm \rightarrow \tau\nu$ (for Type-I, II, L, F), $H^\pm \rightarrow cs$ (for both Type-I and F) and $H^\pm \rightarrow cb$ (Type-F only) survive for light H^\pm . Including the direct search limits for A and H , as shown

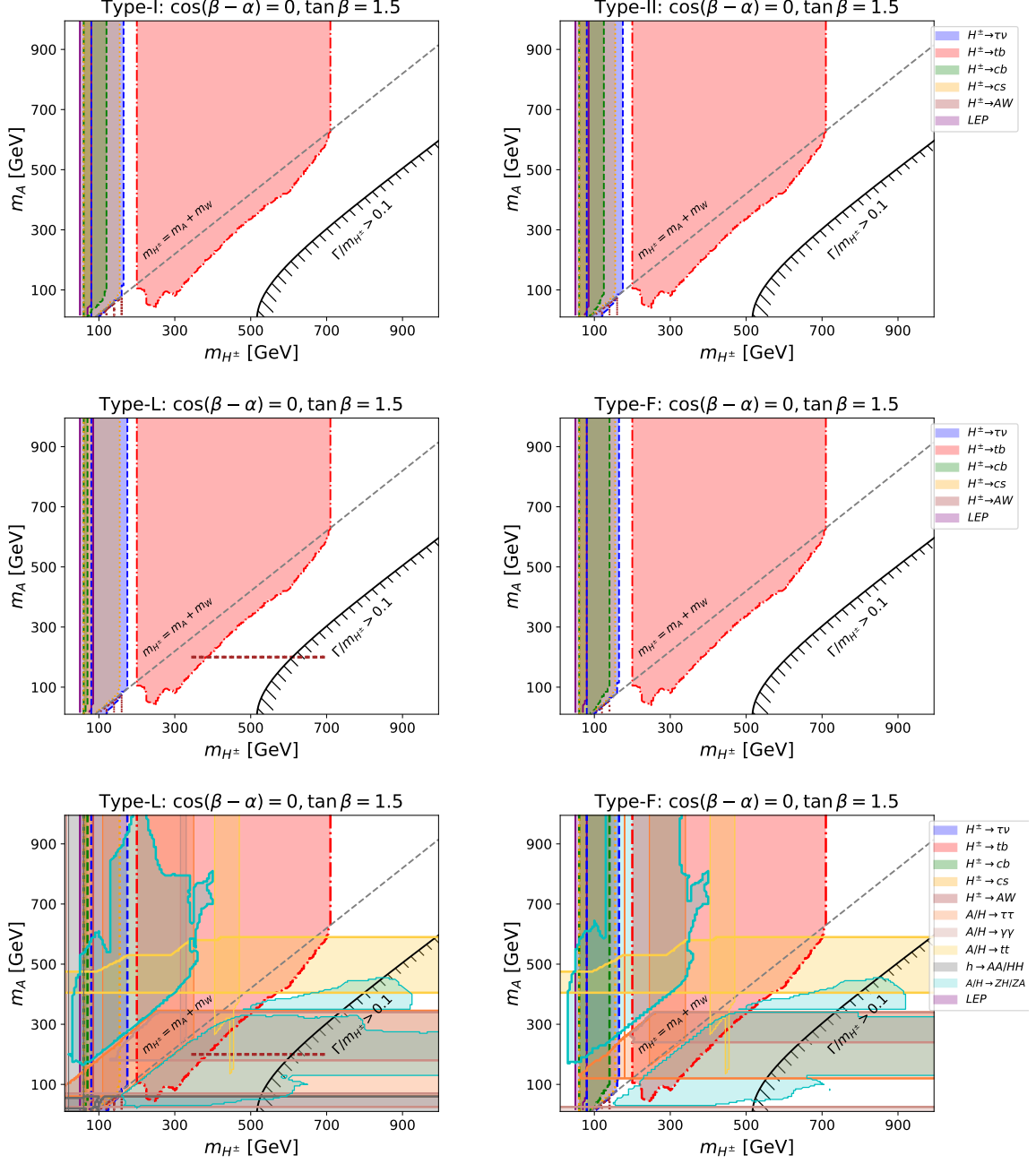


Figure 5. The 95% C.L. exclusion regions in the m_A vs. m_{H^\pm} plane for the Type-I 2HDM (upper left), Type-II 2HDM (upper right), Type-L 2HDM (middle and lower left) and Type-F 2HDM (middle and lower right) for $\tan\beta = 1.5$. In the top four panels, we only show the constraints from H^\pm searches. In the bottom two panels, direct search constraints on the neutral scalar A are included as well. Under the assumption of $m_{H^\pm} = m_H$, we also show regions excluded by the direct searches of H .

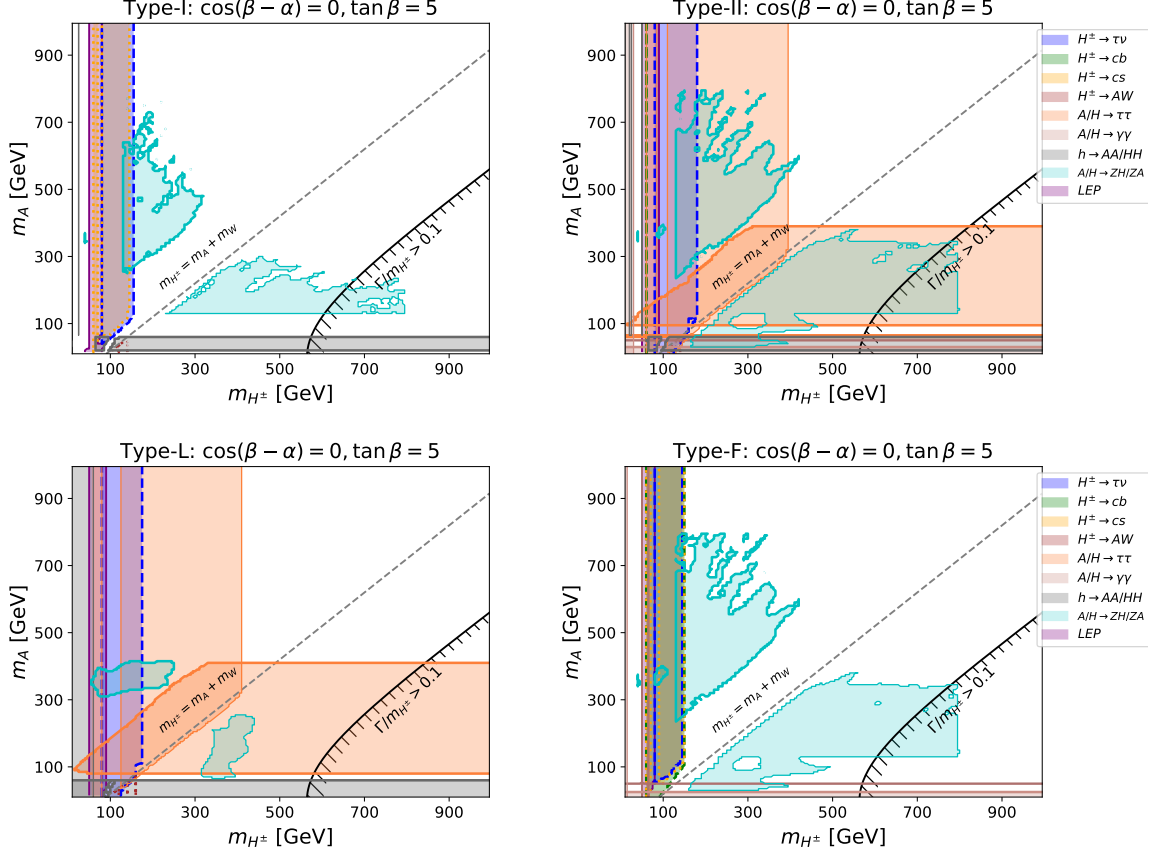


Figure 6. The 95% C.L. exclusions region in the m_A vs. m_{H^\pm} plane in the Type-I 2HDM (upper left), Type-II 2HDM (upper right), Type-L 2HDM (lower left) and Type-F 2HDM (lower right) for $\tan \beta = 5$. Color coding is the same as Figure 5.

in the bottom panels, provides additional limit for the $m_{A,H} < 2m_t$ region. $A/H \rightarrow \tau\tau$ is more effective for the Type-II and Type-L 2HDM, while $A/H \rightarrow HZ/AZ$ are more effective in the Type-I, -II, and -F. Note that the excluded region via $A/H \rightarrow HZ/AZ$ in the Type-L 2HDM is much smaller, since only a weak constraint from $\tau\tau ll$ final states is applicable here. Comparing to the $\tan \beta = 1.5$ case as shown in Fig. 5, $A/H \rightarrow tt$ is absent since tt channel is suppressed at $\tan \beta = 5$.

4.2.3 m_{H^\pm} vs. Δm_A

In Figure 7, we show the current collider limits in the m_{H^\pm} vs. Δm_A plane, with $\tan \beta = 1.5$ for the Type-II and Type-L 2HDM. The results of Type-I, Type-II, Type-L and Type-F 2HDM are nearly identical for small $\tan \beta$ region, except that the constraint provided by the $H^\pm \rightarrow AW$ at heavy m_{H^\pm} is absent in the Type-I, -II, -F. The top-left half of the plane is not physical since it corresponds to $m_A < 0$ GeV. The top-right region at $\Delta m_A \gtrsim 400$ GeV corresponding to large decay width: $\Gamma/m_{H^\pm} > 0.1$, where the resonant searches of H^\pm are not

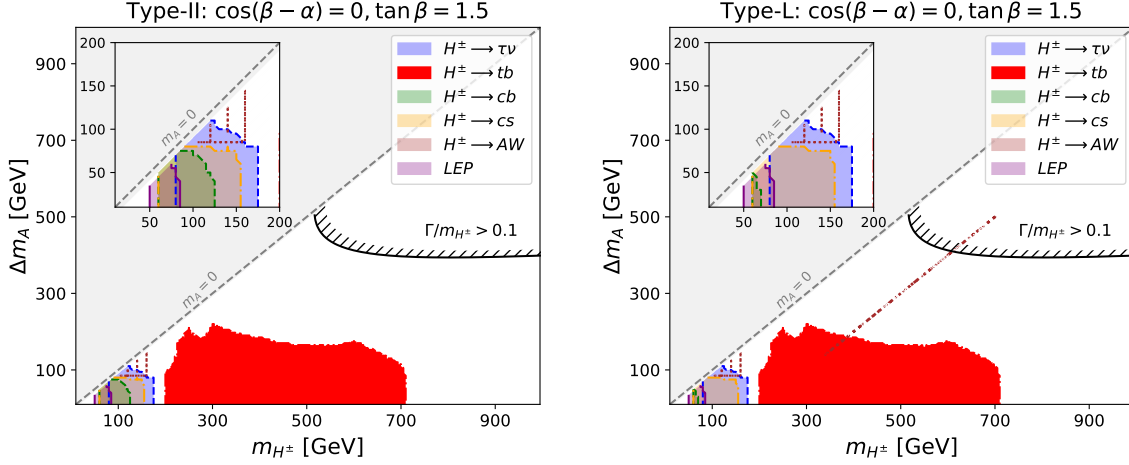


Figure 7. The 95% C.L. exclusion in the $\Delta m_A = m_{H^\pm} - m_A$ vs. m_{H^\pm} plane of the Type-II 2HDM (left) and Type-L 2HDM (right) for $\tan \beta = 1.5$. The upper left corner in each panel shows the zoom-in view of the small mass region. Color coding is the same as Figure 3.

reliable. The reduction of the reach at large $m_{H^\pm} \gtrsim 700$ GeV is mainly due to the decrease of the production cross section at large m_{H^\pm} . Note that $H^\pm \rightarrow AW$ channel is indicated by the horizontal $\Delta m_A = 85$ GeV line and vertical $m_{H^\pm} = 120, 140, 160$ GeV lines in the $m_{H^\pm} < m_t$ region, as well as the $m_A = 200$ GeV line parallel to the diagonal line. For $\Delta m_A < m_W$, the limits are dominated by the fermionic channels of $\tau\nu$, cb , and cs for light m_{H^\pm} and tb for heavy m_{H^\pm} . Once H^\pm decaying to AW is open, the limits from the fermionic channels are relaxed, while $H^\pm \rightarrow AW$ provides the best limit for $\Delta m_A \gtrsim 165$ GeV at $\tan \beta = 1.5$ in the Type-L 2HDM.

We also show the case of $\tan \beta = 50$ for the Type-II (left) and Type-F (right) in Figure 8. At such large value of $\tan \beta$, there is no constraints on the parameter space of the Type-I and Type-L given the suppressed production cross sections. For the Type-II, the parameter space in low mass region is almost entirely excluded by $H^\pm \rightarrow \tau\nu$ and $H^\pm \rightarrow cb$ searches. For the heavy H^\pm , searches for $H^\pm \rightarrow \tau\nu$ and $H^\pm \rightarrow tb$ exclude large range of parameter space with $H^\pm \rightarrow \tau\nu$ dominating. For the Type-F, the parameter space in low mass region is nearly excluded by $H^\pm \rightarrow cs$ and $H^\pm \rightarrow cb$ searches. For the heavy H^\pm , the exclusion range for $H^\pm \rightarrow tb$ is similar to that of the Type-II case, while $H^\pm \rightarrow \tau\nu$ exclusion disappears entirely. Reach of $H^\pm \rightarrow AW$ disappears due to the suppression of the consequent decays of $A \rightarrow \mu\mu, \tau\tau$ at such large $\tan \beta$.

5 Conclusion

After the discovery of the SM-like 125 GeV Higgs, the searches for beyond the SM Higgs bosons became an active experimental search frontier. The 2HDM as one of the simplest extensions of the SM predicts the existence of extra Higgs bosons, including a pair of the

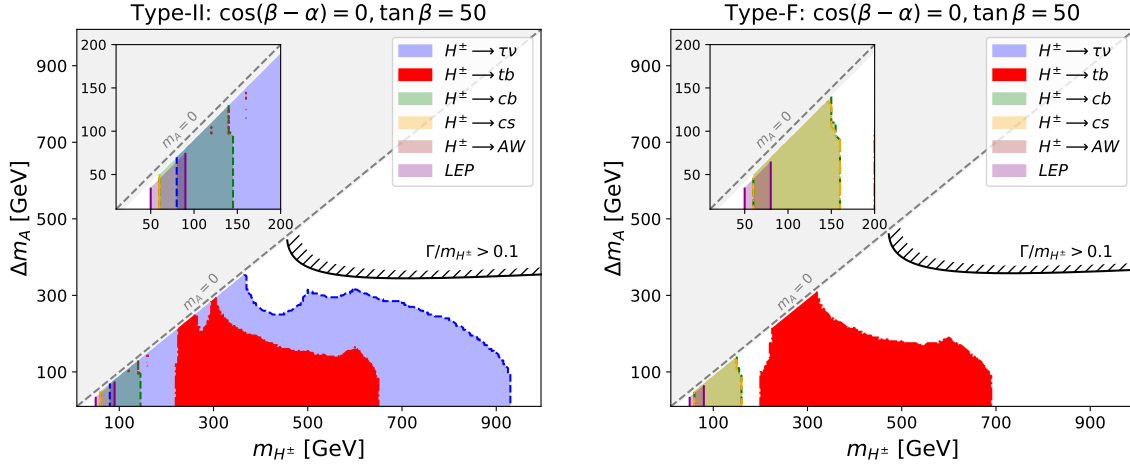


Figure 8. The 95% C.L. exclusion regions in the $\Delta m_A = m_{H^\pm} - m_A$ vs. m_{H^\pm} plane of the Type-II 2HDM (left) and Type-F 2HDM (right) for $\tan \beta = 50$. The upper left corner in each panel shows the zoom-in view of the small mass region. Color coding is the same as Figure 3.

charged Higgses. In this paper we reinterpreted the current search limits of the charged Higgs boson in the four different types of the 2HDM. We considered constraints from Higgs collider searches at the LEP and the LHC, as well as constraints from flavor physics measurements.

Collider searches for the charged Higgses mostly focused on the conventional channels of $\tau\nu$, cs , cb , and tb . When the exotic decay channels of the charged Higgs boson $H^\pm \rightarrow AW/HW$ are open, the constraints from the fermionic channels are relaxed. At the same time, $H^\pm \rightarrow AW/HW$ provide alternative search channels for the charged Higgses, which have been performed at the ATLAS and CMS at 7 TeV, 8 TeV and 13 TeV. In our analyses, we performed a comprehensive study for both the degenerate spectrum of $m_{H^\pm} = m_H = m_A$ as well as the non-degenerate spectrum of $m_{H^\pm} = m_H \neq m_A$, when $H^\pm \rightarrow AW$ open.

For the conventional search channels, the most sensitive detection channel for a light charged Higgs with $m_{H^\pm} < m_t$ is $H^\pm \rightarrow \tau\nu$ and cs . For the Type-I and Type-L, region of $\tan \beta \lesssim 20$ is excluded. For the high mass region of $m_{H^\pm} > m_t$, the most sensitive channel is $H^\pm \rightarrow tb$ with $\tan \beta \lesssim 2$ excluding for a charged Higgs mass up to about 1 TeV. In the Type-II 2HDM, $H^\pm \rightarrow \tau\nu$ provides the strongest constraints at the large $\tan \beta$ region.

When the $H^\pm \rightarrow AW/HW$ decay channels are kinematically available, the constraints from other conventional search channels are weakened. For $m_{H^\pm} < m_t$, $H^\pm \rightarrow AW$ is complementary to the fermionic channels. For the heavy charged Higgs $m_{H^\pm} > m_t$, $H^\pm \rightarrow tb$ still provides the best search limit, except for the Type-L 2HDM, in which $H^\pm \rightarrow AW$ provides the better reach for $1 \lesssim \tan \beta \lesssim 5$. The current experimental search for the exotic channel of $H^\pm \rightarrow AW$ is only performed at a fixed value of $m_A = 200$ GeV. To expand the search of this channel over the entire parameter space of m_{H^\pm} vs. m_A could provide a complementary reach to the $H^\pm \rightarrow tb$ channel.

We also studied the limits in the m_A vs. $m_{H^\pm} = m_H$ plane. At small values of $\tan\beta$, almost the entire parameter space up to $m_{H^\pm} \sim 700$ GeV is excluded below the $H^\pm \rightarrow AW$ threshold with the charged Higgs searches, except a small gap around $m_{H^\pm} \sim m_t$. Once $H^\pm \rightarrow AW$ opens, only the reach from the $H^\pm \rightarrow tb$ channel extends a little bit beyond the threshold. In the Type-L 2HDM, $H^\pm \rightarrow AW$, however, could extend the charged Higgs reach greatly. With the combination of all search channels on both the charged Higgs H^\pm and neutral Higgses H/A , almost the entire region of m_{H^\pm} up to about 700 GeV, and m_A up to about 600 GeV is excluded. The reach, however, is greatly reduced with larger values of $\tan\beta$.

In summary, the exotic charged Higgs search channels $H^\pm \rightarrow AW/HW$ are complementary to the conventional fermionic channels. Extending the current $H^\pm \rightarrow AW/HW$ searches over the entire m_H vs $m_{A,H}$ plane provides great coverage over the $H^\pm \rightarrow tb$ mode. The combination of all the beyond the SM Higgs searches, including both the neutral and charged ones, could provide crucial insights into the extended Higgs sector.

Acknowledgments We would like to thank Adinda De Wit and Alexander Sean Woodcock for insightful discussions. JL and WS are supported by the Natural Science Foundation of China (NSFC) under grant numbers 12305115 and the Shenzhen Science and Technology Program (Grant No. 202206193000001, 20220816094256002). HS is supported by IBS under the project code, IBS-R018-D1. SS is supported by the Department of Energy under Grant No. DEFG02-13ER41976/DE-SC0009913.

References

- [1] **ATLAS** Collaboration, G. Aad et al., *Observation of a new particle in the search for the Standard Model Higgs boson with the ATLAS detector at the LHC*, *Phys. Lett. B* **716** (2012) 1–29, [[arXiv:1207.7214](#)].
- [2] **CMS** Collaboration, S. Chatrchyan et al., *Observation of a New Boson at a Mass of 125 GeV with the CMS Experiment at the LHC*, *Phys. Lett. B* **716** (2012) 30–61, [[arXiv:1207.7235](#)].
- [3] T. D. Lee, *A Theory of Spontaneous T Violation*, *Phys. Rev. D* **8** (1973) 1226–1239.
- [4] G. C. Branco, P. M. Ferreira, L. Lavoura, M. N. Rebelo, M. Sher, and J. P. Silva, *Theory and phenomenology of two-Higgs-doublet models*, *Phys. Rept.* **516** (2012) 1–102, [[arXiv:1106.0034](#)].
- [5] A. Arbey, F. Mahmoudi, O. Stal, and T. Stefaniak, *Status of the Charged Higgs Boson in Two Higgs Doublet Models*, *Eur. Phys. J. C* **78** (2018), no. 3 182, [[arXiv:1706.07414](#)].
- [6] A. G. Akeroyd, *Three body decays of Higgs bosons at LEP-2 and application to a hidden fermiophobic Higgs*, *Nucl. Phys. B* **544** (1999) 557–575, [[hep-ph/9806337](#)].
- [7] A. G. Akeroyd, A. Arhrib, and E. Naimi, *Radiative corrections to the decay $H^+ \rightarrow W^+ A0$* , *Eur. Phys. J. C* **20** (2001) 51–62, [[hep-ph/0002288](#)].
- [8] **ALEPH, DELPHI, L3, OPAL, LEP** Collaboration, G. Abbiendi et al., *Search for Charged Higgs bosons: Combined Results Using LEP Data*, *Eur. Phys. J. C* **73** (2013) 2463, [[arXiv:1301.6065](#)].
- [9] B. Coleppa, F. Kling, and S. Su, *Charged Higgs search via AW^\pm/HW^\pm channel*, *JHEP* **12** (2014) 148, [[arXiv:1408.4119](#)].
- [10] F. Kling, A. Pyarelal, and S. Su, *Light Charged Higgs Bosons to AW/HW via Top Decay*, *JHEP* **11** (2015) 051, [[arXiv:1504.06624](#)].
- [11] H. Bahl, T. Stefaniak, and J. Wittbrodt, *The forgotten channels: charged Higgs boson decays to a W and a non-SM-like Higgs boson*, *JHEP* **06** (2021) 183, [[arXiv:2103.07484](#)].
- [12] F. Kling, H. Li, A. Pyarelal, H. Song, and S. Su, *Exotic Higgs Decays in Type-II 2HDMs at the LHC and Future 100 TeV Hadron Colliders*, *JHEP* **06** (2019) 031, [[arXiv:1812.01633](#)].
- [13] S. Li, H. Song, and S. Su, *Probing Exotic Charged Higgs Decays in the Type-II 2HDM through Top Rich Signal at a Future 100 TeV pp Collider*, *JHEP* **11** (2020) 105, [[arXiv:2005.00576](#)].
- [14] **HFLAV** Collaboration, Y. S. Amhis et al., *Averages of b-hadron, c-hadron, and τ -lepton properties as of 2018*, *Eur. Phys. J. C* **81** (2021), no. 3 226, [[arXiv:1909.12524](#)].
- [15] S. Banerjee et al., *Averages of b-hadron, c-hadron, and τ -lepton properties as of 2023*, [[arXiv:2411.18639](#)].
- [16] **Particle Data Group** Collaboration, S. Navas et al., *Review of particle physics*, *Phys. Rev. D* **110** (2024), no. 3 030001.
- [17] K.-F. Chen, T. Mombächer, and U. de Sanctis, *Analysis of $B_{(s)}^0 \rightarrow \mu^+ \mu^-$ decays at the LHC*, *Symmetry* **16** (2024), no. 2 251, [[arXiv:2402.09901](#)].

- [18] S. Kanemura, M. Kikuchi, and K. Yagyu, *Fingerprinting the extended Higgs sector using one-loop corrected Higgs boson couplings and future precision measurements*, *Nucl. Phys. B* **896** (2015) 80–137, [[arXiv:1502.07716](#)].
- [19] **ATLAS** Collaboration, G. Aad et al., *Search for charged Higgs bosons through the violation of lepton universality in $t\bar{t}$ events using pp collision data at $\sqrt{s} = 7$ TeV with the ATLAS experiment*, *JHEP* **03** (2013) 076, [[arXiv:1212.3572](#)].
- [20] **ATLAS** Collaboration, G. Aad et al., *Search for charged Higgs bosons decaying via $H^+ \rightarrow \tau\nu$ in top quark pair events using pp collision data at $\sqrt{s} = 7$ TeV with the ATLAS detector*, *JHEP* **06** (2012) 039, [[arXiv:1204.2760](#)].
- [21] **ATLAS** Collaboration, G. Aad et al., *Search for charged Higgs bosons decaying via $H^\pm \rightarrow \tau^\pm\nu$ in fully hadronic final states using pp collision data at $\sqrt{s} = 8$ TeV with the ATLAS detector*, *JHEP* **03** (2015) 088, [[arXiv:1412.6663](#)].
- [22] **ATLAS** Collaboration, M. Aaboud et al., *Search for charged Higgs bosons produced in association with a top quark and decaying via $H^\pm \rightarrow \tau\nu$ using pp collision data recorded at $\sqrt{s} = 13$ TeV by the ATLAS detector*, *Phys. Lett. B* **759** (2016) 555–574, [[arXiv:1603.09203](#)].
- [23] **ATLAS** Collaboration, M. Aaboud et al., *Search for charged Higgs bosons decaying via $H^\pm \rightarrow \tau^\pm\nu_\tau$ in the τ +jets and τ +lepton final states with 36 fb^{-1} of pp collision data recorded at $\sqrt{s} = 13$ TeV with the ATLAS experiment*, *JHEP* **09** (2018) 139, [[arXiv:1807.07915](#)].
- [24] **CMS** Collaboration, S. Chatrchyan et al., *Search for a Light Charged Higgs Boson in Top Quark Decays in pp Collisions at $\sqrt{s} = 7$ TeV*, *JHEP* **07** (2012) 143, [[arXiv:1205.5736](#)].
- [25] **CMS** Collaboration, *Search for charged Higgs bosons with the H^\pm to tau nu decay channel in the fully hadronic final state at $\sqrt{s} = 8$ TeV*, tech. rep., CERN, Geneva, 2014.
- [26] **CMS** Collaboration, *Search for a heavy charged Higgs boson in proton-proton collisions at $\sqrt{s} = 8$ TeV with the CMS detector*, tech. rep., CERN, Geneva, 2014.
- [27] **CMS** Collaboration, V. Khachatryan et al., *Search for a charged Higgs boson in pp collisions at $\sqrt{s} = 8$ TeV*, *JHEP* **11** (2015) 018, [[arXiv:1508.07774](#)].
- [28] **CMS** Collaboration, A. M. Sirunyan et al., *Search for charged Higgs bosons in the $H^\pm \rightarrow \tau^\pm\nu_\tau$ decay channel in proton-proton collisions at $\sqrt{s} = 13$ TeV*, *JHEP* **07** (2019) 142, [[arXiv:1903.04560](#)].
- [29] **CMS** Collaboration, *Search for charged Higgs bosons with the $H^\pm \rightarrow \tau^\pm\nu_\tau$ decay channel in the fully hadronic final state at $\sqrt{s} = 13$ TeV*, .
- [30] **ATLAS** Collaboration, G. Aad et al., *Search for a light charged Higgs boson in the decay channel $H^+ \rightarrow c\bar{s}$ in $t\bar{t}$ events using pp collisions at $\sqrt{s} = 7$ TeV with the ATLAS detector*, *Eur. Phys. J. C* **73** (2013) 2465, [[arXiv:1302.3694](#)].
- [31] **CMS** Collaboration, V. Khachatryan et al., *Search for a light charged Higgs boson decaying to $c\bar{s}$ in pp collisions at $\sqrt{s} = 8$ TeV*, *JHEP* **12** (2015) 178, [[arXiv:1510.04252](#)].
- [32] **CMS** Collaboration, A. M. Sirunyan et al., *Search for a light charged Higgs boson in the $H^\pm \rightarrow cs$ channel in proton-proton collisions at $\sqrt{s} = 13$ TeV*, *Phys. Rev. D* **102** (2020) 072001, [[arXiv:2005.08900](#)].
- [33] **ATLAS** Collaboration, G. Aad et al., *Search for a light charged Higgs boson in $t \rightarrow H^\pm b$*

decays, with $H^\pm \rightarrow cs$, in pp collisions at $\sqrt{s} = 13$ TeV with the ATLAS detector, [arXiv:2407.10096](#).

- [34] **ATLAS** Collaboration, G. Aad et al., *Search for a light charged Higgs boson in $t \rightarrow H^\pm b$ decays, with $H^\pm \rightarrow cb$, in the lepton+jets final state in proton-proton collisions at $\sqrt{s} = 13$ TeV with the ATLAS detector*, *JHEP* **09** (2023) 004, [[arXiv:2302.11739](#)].
- [35] **CMS** Collaboration, A. M. Sirunyan et al., *Search for a charged Higgs boson decaying to charm and bottom quarks in proton-proton collisions at $\sqrt{s} = 8$ TeV*, *JHEP* **11** (2018) 115, [[arXiv:1808.06575](#)].
- [36] **ATLAS** Collaboration, G. Aad et al., *Search for charged Higgs bosons in the $H^\pm \rightarrow tb$ decay channel in pp collisions at $\sqrt{s} = 8$ TeV using the ATLAS detector*, *JHEP* **03** (2016) 127, [[arXiv:1512.03704](#)].
- [37] **ATLAS** Collaboration, M. Aaboud et al., *Search for charged Higgs bosons decaying into top and bottom quarks at $\sqrt{s} = 13$ TeV with the ATLAS detector*, *JHEP* **11** (2018) 085, [[arXiv:1808.03599](#)].
- [38] **ATLAS** Collaboration, G. Aad et al., *Search for charged Higgs bosons decaying into a top quark and a bottom quark at $\sqrt{s} = 13$ TeV with the ATLAS detector*, *JHEP* **06** (2021) 145, [[arXiv:2102.10076](#)].
- [39] **CMS** Collaboration, *Search for a heavy charged Higgs boson in proton-proton collisions at $\sqrt{s}=8$ TeV with the CMS detector*, .
- [40] **CMS** Collaboration, A. M. Sirunyan et al., *Search for charged Higgs bosons decaying into a top and a bottom quark in the all-jet final state of pp collisions at $\sqrt{s} = 13$ TeV*, *JHEP* **07** (2020) 126, [[arXiv:2001.07763](#)].
- [41] **CMS** Collaboration, A. M. Sirunyan et al., *Search for a charged Higgs boson decaying into top and bottom quarks in events with electrons or muons in proton-proton collisions at $\sqrt{s} = 13$ TeV*, *JHEP* **01** (2020) 096, [[arXiv:1908.09206](#)].
- [42] **ATLAS** Collaboration, M. Aaboud et al., *Measurements of inclusive and differential fiducial cross-sections of $t\bar{t}$ production with additional heavy-flavour jets in proton-proton collisions at $\sqrt{s} = 13$ TeV with the ATLAS detector*, *JHEP* **04** (2019) 046, [[arXiv:1811.12113](#)].
- [43] **CMS** Collaboration, A. M. Sirunyan et al., *Measurement of the $t\bar{t}b\bar{b}$ production cross section in the all-jet final state in pp collisions at $\sqrt{s} = 13$ TeV*, *Phys. Lett. B* **803** (2020) 135285, [[arXiv:1909.05306](#)].
- [44] **CMS** Collaboration, A. M. Sirunyan et al., *Measurement of the cross section for $t\bar{t}$ production with additional jets and b jets in pp collisions at $\sqrt{s} = 13$ TeV*, *JHEP* **07** (2020) 125, [[arXiv:2003.06467](#)].
- [45] **CMS** Collaboration, A. M. Sirunyan et al., *First measurement of the cross section for top quark pair production with additional charm jets using dileptonic final states in pp collisions at $s=13$ TeV*, *Phys. Lett. B* **820** (2021) 136565, [[arXiv:2012.09225](#)].
- [46] **CMS** Collaboration, *Inclusive and differential cross section measurements of $t\bar{t}b\bar{b}$ production in the lepton+jets channel at $\sqrt{s} = 13$ TeV with the CMS detector*, .
- [47] **CMS** Collaboration, A. Hayrapetyan et al., *Inclusive and differential cross section*

- measurements of $t\bar{t}b\bar{b}$ production in the lepton+jets channel at $\sqrt{s} = 13$ TeV, *JHEP* **05** (2024) 042, [[arXiv:2309.14442](#)].
- [48] **CMS** Collaboration, E. Pfeffer, *Inclusive and differential cross section measurements of $t\bar{t}b\bar{b}$ production in the lepton+jets channel at $\sqrt{s} = 13$ TeV*, in *16th International Workshop on Top Quark Physics*, 1, 2024. [[arXiv:2401.06743](#)].
 - [49] **ATLAS** Collaboration, G. Aad et al., *Measurement of $t\bar{t}$ production in association with additional b-jets in the $e\mu$ final state in proton-proton collisions at $\sqrt{s}=13$ TeV with the ATLAS detector*, [[arXiv:2407.13473](#)].
 - [50] **ATLAS** Collaboration, *Study of $t\bar{t}b\bar{b}$ and $t\bar{t}W$ background modelling for $t\bar{t}H$ analyses*, .
 - [51] **ATLAS** Collaboration, *Studies of Monte Carlo predictions for the $t\bar{t}b\bar{b}$ process*, .
 - [52] L. Ferencz et al., *Study of $t\bar{t}b\bar{b}$ and $t\bar{t}W$ background modelling for $t\bar{t}H$ analyses*, [[arXiv:2301.11670](#)].
 - [53] F. Kling, S. Su, and W. Su, *2HDM Neutral Scalars under the LHC*, *JHEP* **06** (2020) 163, [[arXiv:2004.04172](#)].
 - [54] **CMS** Collaboration, A. M. Sirunyan et al., *Search for a light charged Higgs boson decaying to a W boson and a CP-odd Higgs boson in final states with $e\mu\mu$ or $\mu\mu\mu$ in proton-proton collisions at $\sqrt{s} = 13$ TeV*, *Phys. Rev. Lett.* **123** (2019) 131802, [[arXiv:1905.07453](#)].
 - [55] **ATLAS** Collaboration, *Search for $H^\pm \rightarrow W^\pm A \rightarrow W^\pm \mu\mu$ in $pp \rightarrow t\bar{t}$ events using an $e\mu\mu$ signature with the ATLAS detector at $\sqrt{s} = 13$ TeV*, .
 - [56] **CMS** Collaboration, A. Tumasyan et al., *Search for a charged Higgs boson decaying into a heavy neutral Higgs boson and a W boson in proton-proton collisions at $\sqrt{s} = 13$ TeV*, *JHEP* **09** (2023) 032, [[arXiv:2207.01046](#)].
 - [57] S. Kanemura, *Possible enhancement of the $e^+e^- \rightarrow H^{+-} W^-+$ cross-section in the two Higgs doublet model*, *Eur. Phys. J. C* **17** (2000) 473–486, [[hep-ph/9911541](#)].
 - [58] A. Djouadi, J. Kalinowski, and P. M. Zerwas, *Exploring the SUSY Higgs sector at e^+e^- linear colliders: A Synopsis*, *Z. Phys. C* **57** (1993) 569–584.
 - [59] **ALEPH** Collaboration, A. Heister et al., *Search for charged Higgs bosons in e^+e^- collisions at energies up to $\sqrt{s} = 209$ -GeV*, *Phys. Lett. B* **543** (2002) 1–13, [[hep-ex/0207054](#)].
 - [60] **DELPHI** Collaboration, P. Abreu et al., *Search for charged Higgs bosons at LEP-2*, *Phys. Lett. B* **460** (1999) 484–497.
 - [61] **L3** Collaboration, P. Achard et al., *Search for charged Higgs bosons at LEP*, *Phys. Lett. B* **575** (2003) 208–220, [[hep-ex/0309056](#)].
 - [62] **OPAL** Collaboration, G. Abbiendi et al., *Search for Higgs bosons in e^+e^- collisions at 183-GeV*, *Eur. Phys. J. C* **7** (1999) 407–435, [[hep-ex/9811025](#)].
 - [63] **DELPHI** Collaboration, J. Abdallah et al., *Search for charged Higgs bosons at LEP in general two Higgs doublet models*, *Eur. Phys. J. C* **34** (2004) 399–418, [[hep-ex/0404012](#)].
 - [64] **OPAL** Collaboration, G. Abbiendi et al., *Search for Charged Higgs Bosons in e^+e^- Collisions at $\sqrt{s} = 189 - 209$ GeV*, *Eur. Phys. J. C* **72** (2012) 2076, [[arXiv:0812.0267](#)].

- [65] P. Bechtle, O. Brein, S. Heinemeyer, G. Weiglein, and K. E. Williams, *HiggsBounds: Confronting Arbitrary Higgs Sectors with Exclusion Bounds from LEP and the Tevatron*, *Comput. Phys. Commun.* **181** (2010) 138–167, [[arXiv:0811.4169](#)].
- [66] P. Bechtle, O. Brein, S. Heinemeyer, G. Weiglein, and K. E. Williams, *HiggsBounds 2.0.0: Confronting Neutral and Charged Higgs Sector Predictions with Exclusion Bounds from LEP and the Tevatron*, *Comput. Phys. Commun.* **182** (2011) 2605–2631, [[arXiv:1102.1898](#)].
- [67] P. Bechtle, O. Brein, S. Heinemeyer, O. Stal, T. Stefaniak, G. Weiglein, and K. Williams, *Recent Developments in HiggsBounds and a Preview of HiggsSignals*, *PoS CHARGED2012* (2012) 024, [[arXiv:1301.2345](#)].
- [68] P. Bechtle, O. Brein, S. Heinemeyer, O. Stål, T. Stefaniak, G. Weiglein, and K. E. Williams, *HiggsBounds – 4: Improved Tests of Extended Higgs Sectors against Exclusion Bounds from LEP, the Tevatron and the LHC*, *Eur. Phys. J. C* **74** (2014), no. 3 2693, [[arXiv:1311.0055](#)].
- [69] P. Bechtle, S. Heinemeyer, O. Stal, T. Stefaniak, and G. Weiglein, *Applying Exclusion Likelihoods from LHC Searches to Extended Higgs Sectors*, *Eur. Phys. J. C* **75** (2015), no. 9 421, [[arXiv:1507.06706](#)].
- [70] P. Bechtle, D. Dercks, S. Heinemeyer, T. Klingl, T. Stefaniak, G. Weiglein, and J. Wittbrodt, *HiggsBounds-5: Testing Higgs Sectors in the LHC 13 TeV Era*, *Eur. Phys. J. C* **80** (2020), no. 12 1211, [[arXiv:2006.06007](#)].
- [71] M. Misiak and M. Steinhauser, *Weak radiative decays of the B meson and bounds on M_{H^\pm} in the Two-Higgs-Doublet Model*, *Eur. Phys. J. C* **77** (2017), no. 3 201, [[arXiv:1702.04571](#)].
- [72] M. Misiak, A. Rehman, and M. Steinhauser, *Towards $\bar{B} \rightarrow X_s \gamma$ at the NNLO in QCD without interpolation in m_c* , *JHEP* **06** (2020) 175, [[arXiv:2002.01548](#)].
- [73] O. Atkinson, M. Black, A. Lenz, A. Rusov, and J. Wynne, *Cornering the Two Higgs Doublet Model Type II*, *JHEP* **04** (2022) 172, [[arXiv:2107.05650](#)].
- [74] M. Czaaja and M. Misiak, *Symmetry* **16** (2024) no.7, 917 doi:10.3390/sym16070917 [[arXiv:2407.03810 \[hep-ph\]](#)].
- [75] F. Mahmoudi, *SuperIso v3.0, flavor physics observables calculations: Extension to NMSSM*, *Comput. Phys. Commun.* **180** (2009) 1718–1719.
- [76] F. Mahmoudi, *SuperIso v2.3: A Program for calculating flavor physics observables in Supersymmetry*, *Comput. Phys. Commun.* **180** (2009) 1579–1613, [[arXiv:0808.3144](#)].
- [77] F. Mahmoudi, *SuperIso: A Program for calculating the isospin asymmetry of $B \rightarrow K^* \gamma$ in the MSSM*, *Comput. Phys. Commun.* **178** (2008) 745–754, [[arXiv:0710.2067](#)].
- [78] **ALEPH, DELPHI, L3, OPAL, SLD, LEP Electroweak Working Group, SLD Electroweak Group, SLD Heavy Flavour Group** Collaboration, S. Schael et al., *Precision electroweak measurements on the Z resonance*, *Phys. Rept.* **427** (2006) 257–454, [[hep-ex/0509008](#)].
- [79] F. Kling, J. M. No, and S. Su, *Anatomy of Exotic Higgs Decays in 2HDM*, *JHEP* **09** (2016) 093, [[arXiv:1604.01406](#)].
- [80] W. Beenakker, R. Hopker, and M. Spira, *PROSPINO: A Program for the production of supersymmetric particles in next-to-leading order QCD*, [hep-ph/9611232](#).

- [81] T. Plehn, *Charged Higgs boson production in bottom gluon fusion*, *Phys. Rev. D* **67** (2003) 014018, [[hep-ph/0206121](#)].
- [82] D. Eriksson, J. Rathsman, and O. Stal, *2HDMC: Two-Higgs-Doublet Model Calculator Physics and Manual*, *Comput. Phys. Commun.* **181** (2010) 189–205, [[arXiv:0902.0851](#)].
- [83] **CMS** Collaboration, A. M. Sirunyan et al., *Search for additional neutral MSSM Higgs bosons in the $\tau\tau$ final state in proton-proton collisions at $\sqrt{s} = 13$ TeV*, *JHEP* **09** (2018) 007, [[arXiv:1803.06553](#)].
- [84] **CMS** Collaboration, A. M. Sirunyan et al., *Search for a low-mass $\tau^+\tau^-$ resonance in association with a bottom quark in proton-proton collisions at $\sqrt{s} = 13$ TeV*, *JHEP* **05** (2019) 210, [[arXiv:1903.10228](#)].
- [85] **ATLAS** Collaboration, G. Aad et al., *Search for heavy Higgs bosons decaying into two tau leptons with the ATLAS detector using pp collisions at $\sqrt{s} = 13$ TeV*, *Phys. Rev. Lett.* **125** (2020), no. 5 051801, [[arXiv:2002.12223](#)].
- [86] **CMS** Collaboration, A. Tumasyan et al., *Searches for additional Higgs bosons and for vector leptoquarks in $\tau\tau$ final states in proton-proton collisions at $\sqrt{s} = 13$ TeV*, *JHEP* **07** (2023) 073, [[arXiv:2208.02717](#)].
- [87] **CMS** Collaboration, A. Hayrapetyan et al., *Search for new physics in high-mass diphoton events from proton-proton collisions at $\sqrt{s} = 13$ TeV*, *JHEP* **08** (2024) 215, [[arXiv:2405.09320](#)].
- [88] G. Aad et al. [ATLAS], *JHEP* **07** (2023), 155 doi:10.1007/JHEP07(2023)155 [[arXiv:2211.04172](#) [hep-ex]].
- [89] **ATLAS** Collaboration, *Search for resonances in the 65 to 110 GeV diphoton invariant mass range using 80 fb⁻¹ of pp collisions collected at $\sqrt{s} = 13$ TeV with the ATLAS detector*, .
- [90] **ATLAS** Collaboration, M. Aaboud et al., *Search for new phenomena in high-mass diphoton final states using 37 fb⁻¹ of proton-proton collisions collected at $\sqrt{s} = 13$ TeV with the ATLAS detector*, *Phys. Lett. B* **775** (2017) 105–125, [[arXiv:1707.04147](#)].
- [91] **ATLAS** Collaboration, G. Aad et al., *Search for Scalar Diphoton Resonances in the Mass Range 65 – 600 GeV with the ATLAS Detector in pp Collision Data at $\sqrt{s} = 8$ TeV*, *Phys. Rev. Lett.* **113** (2014), no. 17 171801, [[arXiv:1407.6583](#)].
- [92] **CMS** Collaboration, A. M. Sirunyan et al., *Search for a standard model-like Higgs boson in the mass range between 70 and 110 GeV in the diphoton final state in proton-proton collisions at $\sqrt{s} = 8$ and 13 TeV*, *Phys. Lett. B* **793** (2019) 320–347, [[arXiv:1811.08459](#)].
- [93] **CMS** Collaboration, A. M. Sirunyan et al., *Search for physics beyond the standard model in high-mass diphoton events from proton-proton collisions at $\sqrt{s} = 13$ TeV*, *Phys. Rev. D* **98** (2018), no. 9 092001, [[arXiv:1809.00327](#)].
- [94] **ATLAS** Collaboration, G. Aad et al., *Search for heavy neutral Higgs bosons decaying into a top quark pair in 140 fb⁻¹ of proton-proton collision data at $\sqrt{s} = 13$ TeV with the ATLAS detector*, *JHEP* **08** (2024) 013, [[arXiv:2404.18986](#)].
- [95] **CMS** Collaboration, A. M. Sirunyan et al., *Search for heavy Higgs bosons decaying to a top quark pair in proton-proton collisions at $\sqrt{s} = 13$ TeV*, *JHEP* **04** (2020) 171, [[arXiv:1908.01115](#)]. [Erratum: *JHEP* 03, 187 (2022)].

- [96] **ATLAS** Collaboration, G. Aad et al., *Search for Higgs boson decays into a pair of pseudoscalar particles in the $b\bar{b}\mu\mu$ final state with the ATLAS detector in pp collisions at $\sqrt{s}=13$ TeV*, *Phys. Rev. D* **105** (2022), no. 1 012006, [[arXiv:2110.00313](#)].
- [97] **CMS** Collaboration, A. M. Sirunyan et al., *Search for a light pseudoscalar Higgs boson in the boosted $\mu\mu\tau\tau$ final state in proton-proton collisions at $\sqrt{s} = 13$ TeV*, *JHEP* **08** (2020) 139, [[arXiv:2005.08694](#)].
- [98] **CMS** Collaboration, A. Tumasyan et al., *Search for low-mass dilepton resonances in Higgs boson decays to four-lepton final states in proton-proton collisions at $\sqrt{s} = 13$ TeV*, *Eur. Phys. J. C* **82** (2022), no. 4 290, [[arXiv:2111.01299](#)].
- [99] **CMS** Collaboration, A. Tumasyan et al., *Search for the exotic decay of the Higgs boson into two light pseudoscalars with four photons in the final state in proton-proton collisions at $\sqrt{s} = 13$ TeV*, *JHEP* **07** (2023) 148, [[arXiv:2208.01469](#)].
- [100] **CMS** Collaboration, A. Tumasyan et al., *Search for exotic Higgs boson decays $H \rightarrow \mathcal{A}\mathcal{A} \rightarrow 4\gamma$ with events containing two merged diphotons in proton-proton collisions at $\sqrt{s} = 13$ TeV*, *Phys. Rev. Lett.* **131** (2023) 101801, [[arXiv:2209.06197](#)].
- [101] **CMS** Collaboration, A. Hayrapetyan et al., *Search for the decay of the Higgs boson to a pair of light pseudoscalar bosons in the final state with four bottom quarks in proton-proton collisions at $\sqrt{s} = 13$ TeV*, *JHEP* **06** (2024) 097, [[arXiv:2403.10341](#)].
- [102] **CMS** Collaboration, A. M. Sirunyan et al., *A search for pair production of new light bosons decaying into muons in proton-proton collisions at 13 TeV*, *Phys. Lett. B* **796** (2019) 131–154, [[arXiv:1812.00380](#)].
- [103] **ATLAS** Collaboration, M. Aaboud et al., *Search for Higgs boson decays to beyond-the-Standard-Model light bosons in four-lepton events with the ATLAS detector at $\sqrt{s} = 13$ TeV*, *JHEP* **06** (2018) 166, [[arXiv:1802.03388](#)].
- [104] **CMS** Collaboration, A. M. Sirunyan et al., *Search for an exotic decay of the Higgs boson to a pair of light pseudoscalars in the final state of two muons and two τ leptons in proton-proton collisions at $\sqrt{s} = 13$ TeV*, *JHEP* **11** (2018) 018, [[arXiv:1805.04865](#)].
- [105] **ATLAS** Collaboration, G. Aad et al., *Search for Higgs bosons decaying to aa in the $\mu\mu\tau\tau$ final state in pp collisions at $\sqrt{s} = 8$ TeV with the ATLAS experiment*, *Phys. Rev. D* **92** (2015), no. 5 052002, [[arXiv:1505.01609](#)].
- [106] **CMS** Collaboration, A. M. Sirunyan et al., *Search for light pseudoscalar boson pairs produced from decays of the 125 GeV Higgs boson in final states with two muons and two nearby tracks in pp collisions at $\sqrt{s} = 13$ TeV*, *Phys. Lett. B* **800** (2020) 135087, [[arXiv:1907.07235](#)].
- [107] **CMS** Collaboration, A. M. Sirunyan et al., *Search for an exotic decay of the Higgs boson to a pair of light pseudoscalars in the final state with two muons and two b quarks in pp collisions at 13 TeV*, *Phys. Lett. B* **795** (2019) 398–423, [[arXiv:1812.06359](#)].
- [108] **ATLAS** Collaboration, M. Aaboud et al., *Search for Higgs boson decays into a pair of light bosons in the $b\bar{b}\mu\mu$ final state in pp collision at $\sqrt{s}=13$ TeV with the ATLAS detector*, *Phys. Lett. B* **790** (2019) 1–21, [[arXiv:1807.00539](#)].
- [109] **CMS** Collaboration, A. M. Sirunyan et al., *Search for an exotic decay of the Higgs boson to a*

pair of light pseudoscalars in the final state with two b quarks and two τ leptons in proton-proton collisions at $\sqrt{s} = 13$ TeV, *Phys. Lett. B* **785** (2018) 462, [[arXiv:1805.10191](#)].

- [110] **ATLAS** Collaboration, M. Aaboud et al., *Search for the Higgs boson produced in association with a vector boson and decaying into two spin-zero particles in the $H \rightarrow aa \rightarrow 4b$ channel in pp collisions at $\sqrt{s} = 13$ TeV with the ATLAS detector*, *JHEP* **10** (2018) 031, [[arXiv:1806.07355](#)].
- [111] **CMS** Collaboration, V. Khachatryan et al., *Search for neutral resonances decaying into a Z boson and a pair of b jets or τ leptons*, *Phys. Lett. B* **759** (2016) 369–394, [[arXiv:1603.02991](#)].
- [112] **ATLAS** Collaboration, M. Aaboud et al., *Search for a heavy Higgs boson decaying into a Z boson and another heavy Higgs boson in the $\ell\ell b\bar{b}$ final state in pp collisions at $\sqrt{s} = 13$ TeV with the ATLAS detector*, *Phys. Lett. B* **783** (2018) 392–414, [[arXiv:1804.01126](#)].
- [113] **CMS** Collaboration, A. M. Sirunyan et al., *Search for new neutral Higgs bosons through the $H \rightarrow ZA \rightarrow \ell^+ \ell^- b\bar{b}$ process in pp collisions at $\sqrt{s} = 13$ TeV*, *JHEP* **03** (2020) 055, [[arXiv:1911.03781](#)].
- [114] **ATLAS** Collaboration, G. Aad et al., *Search for a heavy Higgs boson decaying into a Z boson and another heavy Higgs boson in the $\ell\ell b\bar{b}$ and $\ell\ell WW$ final states in pp collisions at $\sqrt{s} = 13$ TeV with the ATLAS detector*, *Eur. Phys. J. C* **81** (2021), no. 5 396, [[arXiv:2011.05639](#)].
- [115] **ATLAS** Collaboration, *Search for a CP-odd Higgs boson decaying to a heavy CP-even Higgs boson and a Z boson in the $\ell\ell t\bar{t}$ and $\nu\bar{\nu} b\bar{b}$ final states using 140 fb^{-1} of data collected with the ATLAS detector*, .
- [116] **ATLAS** Collaboration, G. Aad et al., *Search for Higgs boson pair production in association with a vector boson in pp collisions at $\sqrt{s} = 13$ TeV with the ATLAS detector*, *Eur. Phys. J. C* **83** (2023), no. 6 519, [[arXiv:2210.05415](#)].